Characterization of Surface Micro-Roughness by Off-Specular Measurements of Polarized Optical Scattering

Cheng-Yang Liu, Li-Jen Chang

Department of Biomedical Engineering, National Yang-Ming University, Taipei City, Taiwan, cyliu66@ym.edu.tw

The characterization of surface micro-roughness is investigated by using off-specular measurements of polarized optical scattering. In the measurement system, the detection angles of optical scattering are defined by the vertical and level scattering angles. The rotating mechanism of angles is controlled by stepper motors. Waveplate and polarizer are used to adjust light polarization and detection. We conduct the optical scattering measurements by using four standard metal sheets of surface roughness. The nominal values (Ra) of standard micro-roughness are 1.6 μm, 0.8 μm, 0.4 μm, and 0.1 μm, respectively. Samples with different surface roughness are evaluated with the utilization of laser sources at three incident wavelengths. These polarized images are analyzed using a computer program to obtain the distribution of light intensity. The results show great correlation between the metal surface roughness and polarization states. This measurement system can be used to quickly and accurately distinguish between different surfaces and properties.

Keywords: Optical scattering, polarization, micro-roughness.

1. INTRODUCTION

There are many techniques for surface inspection, among which noncontact measurements are the most important for application. Optical scattering experiments provide many messages on the sample materials, such as their optical characteristics and surface features. The optical scattering measurement methods have been proposed in many references [1]-[6]. The most conventional method is in-plane light-scattering measurement. The scattering angles are defined by the incident light and reflected light in a plane. Polarized light-scattering analysis, which is an accurate optical method, is used in the in-plane measurement. The information of surface roughness can be obtained by polarized light-scattering analysis. According to the Stokes theory, polarization is considered as one of the states of electromagnetic wave. The different surface roughnesses can be distinguished from different conditions of scattered light [7]. The capability of polarized optical scattering measurement promises a wide range of application including characteristic detection of skin tissue for medical use. This measurement method obtains hidden information from the surface that cannot be acquired by human eyes. In medical science, the polarized imaging measurement has proved its precision and reliability [8], [9].

By using two-axis scatterometry, the relationship between simple surface characteristics and polarized light-scattering is determined. However, two-axis scatterometry methods have several disadvantages. The measuring range is limited by in-plane measurement. It only observes in-plane information of light-scattering and the experimental results are not applicable for real surface. In order to overcome these disadvantages, three-axis scatterometry can be employed for accurately detecting the complex surface roughness. Many researchers have started to develop three-axis scatterometry systems and to delimit geometric light on hemisphere [10]-[27]. The depolarization and distribution of scattered light in off-specular reflection by rough surfaces are studied. The light depolarization by an oriented rough surface relates to its roughness and material property. In the system, stepper motors are used to control the incident and the out-of-plane detecting angles. By exploiting this knowledge, the improvements can be made in the detection of small particle or surface roughness. The measured images are analyzed by using the Muller matrix which gives the relationship between polarization state and surface roughness. The condition of surface roughness can thus be obtained from the experimental data. The bidirectional reflectance distribution function (BRDF) is used to define reflected light at an opaque surface. It has been confirmed that the BRDF method is accurate and practical in scattered light measurement. Furthermore, speckle image systems are similar to two-axis scatterometry systems, but the amount of information obtained is less than that in three-axis scatterometry [28], [29]. Speckle pattern can evaluate the value of surface roughness but cannot display a clear surface image [30]-[36]. Information collected by two-axis scatterometry is limited, and a three-axis scatterometry system has to be developed.

In this paper, the off-specular measurements from metal surfaces are achieved by the polarized optical scattering measurement system. The wavelengths of the incident light adopted in this system are 405 nm, 515 nm, and 671 nm. The light beam is applied to standard sheets with different surface roughness for acquiring polarized images. From the polarized images, the relationship between polarization states and surface roughness is calculated by using the matrix analysis. This study also obtains the slope of mean degree of linear polarization on different surface roughness. This experimental system is proved to be fast and accurate in obtaining clear polarized scattering images of surface. The details of experiment are introduced carefully in this article.

2. EXPERIMENTAL METHODS

Theories for light scattering from surface roughness have been developed elsewhere [2]-[7]. The theoretical description in this paper is used to support the experimental method of light scattering. In practice, the theoretical approach has problems to distinguish the value of surface roughness because the roughness is usually non-uniform distribution on the surface in a large area. For roughness-induced scatter in the smooth surface limit, the results of first-order vector perturbation theory are summarized here briefly [3], [4], [7]. The surface roughness of the standard sheets is measured by using out-of-plane measurement of optical scattering. Fig.1. shows the incident and detecting angles for a surface micro-roughness. The incident angle of the polarized beam is defined as θ_i in X-Z plane and the out-of-plane angle is defined as ϕ_i. The scattered light has a reflection angle θ_r with the Z axis. When polarized light irradiates onto a standard sheet, it produces scattering light in the hemisphere. The BRDF is defined as a function of optical scattering from a surface [12], as follows:

$$f(\theta_i, \phi_i, \theta_r, \phi_r) = \frac{\partial \sigma_r}{\partial \omega} \frac{1}{\sigma_i \cos \theta_r} \tag{1}$$

where $\partial \sigma_r / \partial \omega$ is scattered intensity per unit solid angle. σ_i is the power of the light. θ_i and θ_r are the polar angles of incident and reflected beam. ϕ_i and ϕ_r are azimuth of incident and scattered light. The Jones matrix of scattered light from a sample surface is expressed as follows [7]:

$$\begin{pmatrix} E_p^{scat} \\ E_s^{scat} \end{pmatrix} = \frac{\exp(ikR)}{R} \begin{pmatrix} q_{pp} & q_{sp} \\ q_{ps} & q_{ss} \end{pmatrix} \begin{pmatrix} E_p^{inc} \\ E_s^{inc} \end{pmatrix} \tag{2}$$

where $k = 2\pi/\lambda$, λ is the wavelength of laser, R is the distance from the scattered light to detector, and q_{ij} are as follows:

$$q_{ss} = \frac{(n_{sur}^2-1)\cos\phi_r}{[\cos\theta_i+(n_{sur}^2-\sin^2\theta_i)^{1/2}][\cos\theta_r+(n_{sur}^2-\sin^2\theta_r)^{1/2}]}$$

$$q_{sp} = \frac{-(n_{sur}^2-1)\sin\phi_r(n_{sur}^2-\sin^2\theta_r)^{1/2}}{[\cos\theta_i+(n_{sur}^2-\sin^2\theta_i)^{1/2}][n_{sur}^2\cos\theta_r+(n_{sur}^2-\sin^2\theta_r)^{1/2}]}$$

$$q_{ps} = \frac{-(n_{sur}^2-1)\sin\phi_r(n_{sur}^2-\sin^2\theta_i)^{1/2}}{[n_{sur}^2\cos\theta_i+(n_{sur}^2-\sin^2\theta_i)^{1/2}][\cos\theta_r+(n_{sur}^2-\sin^2\theta_r)^{1/2}]}$$

$$q_{pp} = \frac{(n_{sur}^2-1)[n_{sur}^2\sin\theta_i\sin\theta_r-(n_{sur}^2-\sin^2\theta_i)^{1/2}(n_{sur}^2-\sin^2\theta_r)^{1/2}\cos\phi_r]}{[n_{sur}^2\cos\theta_i+(n_{sur}^2-\sin^2\theta_i)^{1/2}][n_{sur}^2\cos\theta_r+(n_{sur}^2-\sin^2\theta_r)^{1/2}]} \tag{3}$$

where n_{sur} is the refractive index of the surface material.

In the experiment, θ_i and θ_r are set at a fixed angle (45° or 60°) and ϕ_i is 180°. The ϕ_r rotates from 0° to 180° in every 5°. A mechanism is designed for controlling the rotation of the standard sheet in four directions. The standard sheet rotates at different angles and then a charge coupled device (CCD) detects the intensity of the scattered light. The scattered light from a surface roughness of these standard sheets can hence be measured and recorded on a hemisphere. Specific reports of optical scattering by a surface characteristic have been presented in many academic publications [1]-[20]. According to the participation of these literatures, the optical scattering principle is described briefly here. In order to evaluate measurement data from multi-direction immediately, the out-of-plane optical scattering coordinate system is illustrated in Fig.1. to describe the angular dependence of a scattered field from a surface. A polarized laser beam is illuminating a surface at an incident polar angle θ_i. The orientation of scattered light is clarified by a polar angle θ_r and an azimuth angle ϕ_r.
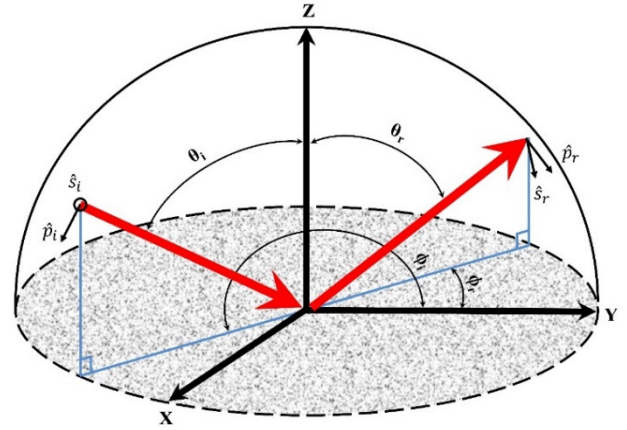

Fig.1. Out-of-plane optical scattering coordinate system for a surface micro-roughness.

The polarized scattering measurement system is employed to study off-specular optical scattering from a surface micro-roughness. Fig.2. depicts the experimental apparatus of the polarized scattering measurement system. Fig.2.a) shows the multi-axis rotating mechanism controlled by stepper motors for four rotation angles. The CCD rotates 360° around the sample. The sample holder performs full rotation with respect to a horizontal axis and a vertical axis. The sample holder also revolves on its own axis. The angles of the incident light and the detection angles of the scattered light can be adjusted by the four stepper motors. By suitably adjusting the angles of rotation, we can effectively detect the scattered light produced by the surface roughness. Fig.2.b) shows the light source assembly which consists of laser, pinhole, filter, waveplate, polarizer, spatial filter system, and beam expander. Because the different wavelengths have varied effects on surface roughness, three incident wavelengths (405 nm, 515 nm, and 671 nm) of laser are chosen for measurements. To ensure that the laser provides the required angle of polarization, waveplate and polarizer are adopted to

adjust the direction of polarization. The uniform laser source is enlarged by beam expander. The incident laser with linear polarization is collimated and the diameter of the laser beam is about 3 cm. Fig.2.c) shows the detecting components which include polarizer, TV zoom lens, and CCD. The polarizer is set up in front of the detector, which controls the polarization of the received light. The image is focused by TV zoom lens and the CCD receives scattering light from the surface at different angles. The hemispherical imaging of optical scattering can be accomplished by the polarized scattering measurement system.
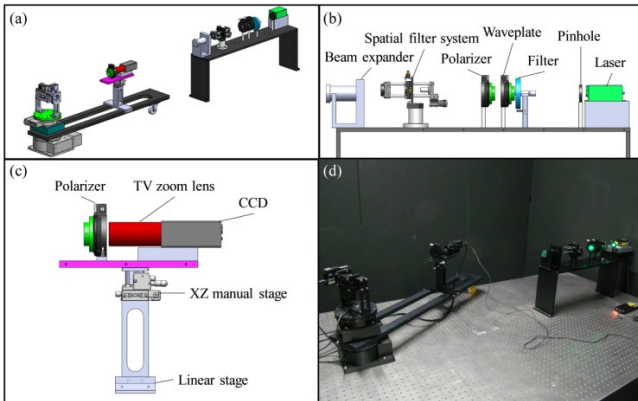

Fig.2. The polarized scattering measurement system: a) overall schematic diagram, b) light source assembly, c) detecting components, and d) photograph.

3. EXPERIMENTAL RESULTS AND ANALYSES

For estimating the polarized imaging from a surface micro-roughness, the four standard sheets are sliced from the surface roughness standard sets (Flexbar 16008). The standard sheets are made of solid electroformed nickel and random rough surfaces by grinding. The metal standard sheets (Flexbar 16008) of surface roughness of 1.6 μm, 0.8 μm, 0.4 μm, and 0.1 μm are used. The complex indices of refraction of nickel are assumed to be 1.61+2.36i at 405 nm, 1.71+3.06i at 515 nm, and 2.08+3.91i at 671 nm [37]. A stylus profiler (Kosaka ET4100) is performed on each of the standard sheets for comparison. The average values of roughness are measured to be Ra = 1.526 μm, Ra = 0.712 μm, Ra = 0.368 μm, and Ra = 0.173 μm for the nominal values of 1.6 μm, 0.8 μm, 0.4 μm, and 0.1 μm, respectively. Fig.3. shows the four standard sheets at different surface roughnesses. In this part, the off-specular measurements for the standard sheets are described.
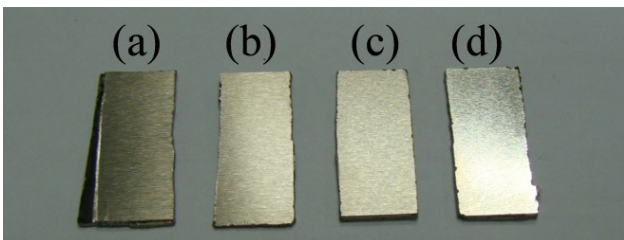

Fig.3. Standard sheets of surface micro-roughness: a) Ra = 1.6 μm, b) Ra = 0.8 μm, c) Ra = 0.4 μm, and d) Ra = 0.1 μm.

The optical scattering from the surface features is determined by the property of the Jones matrix. The equivalent intensity relationship is expressed using the Stokes-Mueller representation via the BRDF. The polarization states of optical scattering can be represented by a Stokes vector [7]. The element of a Stokes vector is characterized as Φ_j (j = 0, 1, 2, 3). The first three elements of a Stokes vector correspond to linear states of polarization. The polarization states can be indicated by the principal angle and the degree of linear polarization. The principal angle is defined as $\eta = 1/2 \arctan(\Phi_2/\Phi_1)$. By facing the laser, the principal angle is estimated counterclockwise with respect to the horizontal axis. The degree of linear polarization P_L is described by

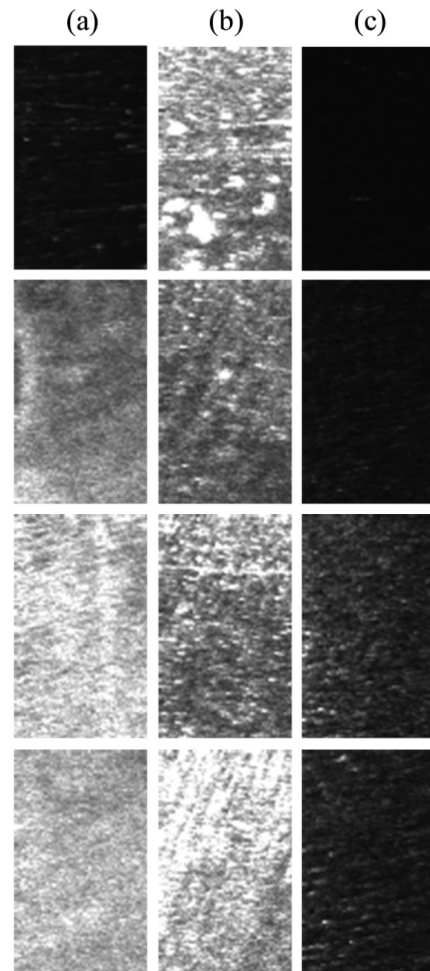$$P_L = \frac{\sqrt{\Phi_1^2 + \Phi_2^2}}{\Phi_0} \qquad (4)$$

Fig.4. PP images for surface roughnesses of Ra = 0.1 μm (the first row), Ra = 0.4 μm (the second row), Ra = 0.8 μm (the third row), and Ra = 1.6 μm (the fourth row) at a) λ = 405 nm and $\phi_r = 35°$, b) λ = 515 nm and $\phi_r = 155°$, and c) λ = 671 nm and $\phi_r = 20°$.

$P_L = 1$ means linear polarization and $P_L = 0$ means unpolarized light or circular polarization. The linear polarization P_L and principal angle η entirely describe the

polarization states of optical scattering and are derived simply from partial Stokes vector. Our experimental apparatus contains two polarizers. The incident beam is polarized with the first polarizer oriented parallel (P) to the X-Y plane. The second polarizer (analyzer) is mounted on a rotational stage in front of the camera in order to detect three polarization states: parallel (P), perpendicular (S), and 45° (P45) to the X-Y plane. We demand three polarized images for polarized calculations. When the main axis of analyzer is parallel with the X-Y plane, the PP image is received. The PS image is received when the main axis of analyzer is perpendicular to the X-Y plane. Finally, the P45 image is received when the main axis of analyzer is oriented to the X-Y plane at 45°. The polarized optical scattering image (POSI) is expressed as POSI = (PP-PS) / (PP+PS). Since the POSI is normalized to the sum of PP and PS, the variety of laser source and the impact of superficial imperfections are removed. Besides, the influence of the multiply photon scattering in the POSI is also removed by deducting PS from PP. In equation (4), these elements of a partial Stokes vector are described as

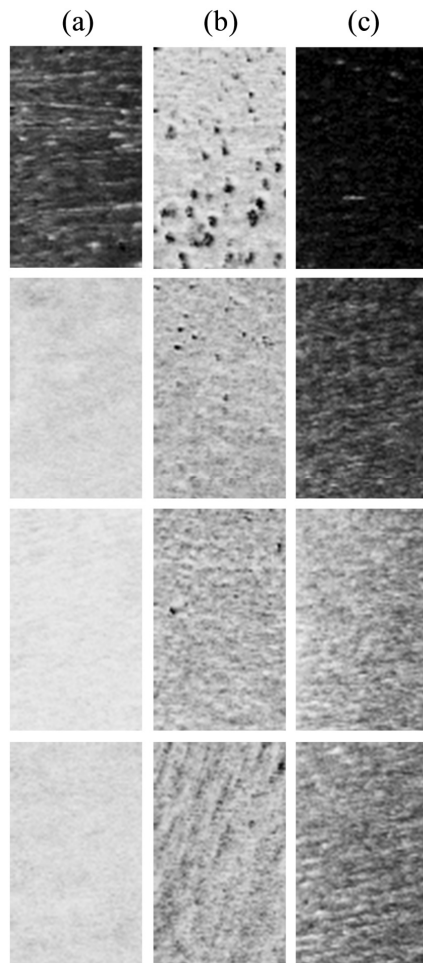$$\Phi_0 = 2PS + 2PP, \quad \Phi_1 = 2PS - 2PP, \quad \Phi_2 = 4P45 - 2PS - 2PP \quad (5)$$

The polarization behavior is very responsive to the scattering mechanism from a surface. Fig.4. shows the PP images for surface roughnesses of Ra = 0.1 μm (the first row), Ra = 0.4 μm (the second row), Ra = 0.8 μm (the third row), and Ra = 1.6 μm (the fourth row) at different incident wavelengths and measuring angles. It can be seen that the clear PP images are obtained at λ = 515 nm and ϕ_r = 155° for all surface roughnesses. However, the blurred PP images are observed at λ = 671 nm and ϕ_r = 20°. Optical backscattering from surface roughness keeps the direction of laser polarization and affects the PP image intensely. The multiply scattering is from deep surface layers and affects the PP and PS images equally. Fig.5. shows the POSI images for Ra = 0.1 μm (the first row), Ra = 0.4 μm (the second row), Ra = 0.8 μm (the third row), and Ra = 1.6 μm (the fourth row) at different incident wavelengths and measuring angles. These POSI images intimate that the micro-roughness strongly effects distinct intensity distributions of optical scattering. The surface texture and defects are clearly observed in the POSI images at λ = 515 nm and ϕ_r = 155°. The multiple surface diffusion is eliminated by choosing incident wavelength λ and azimuth angle ϕ_r appropriately. The POSI image is produced by merging the advantages of the PP and PS images at different measured conditions which shows significant surface roughness.
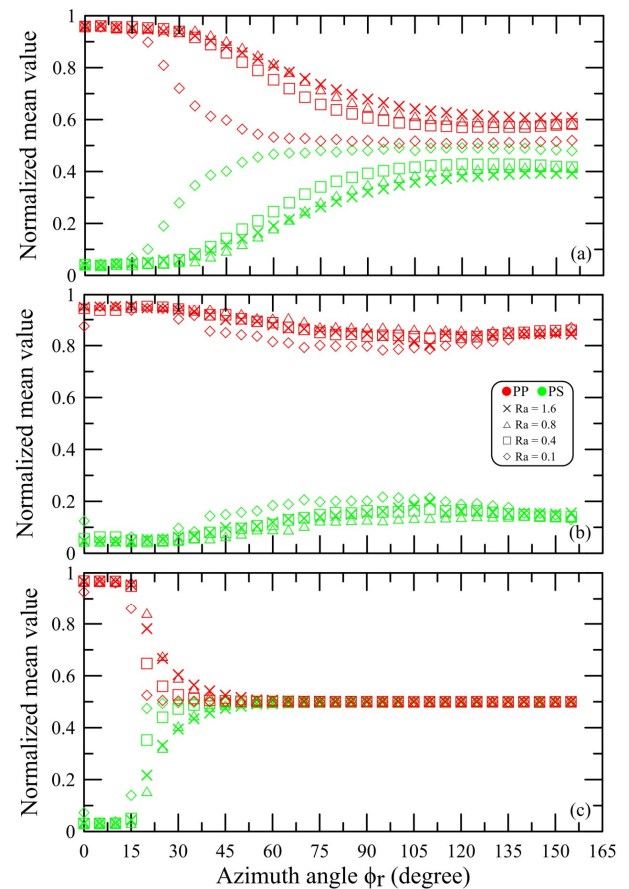

Fig.5. POSI images for of Ra = 0.1 μm (the first row), Ra = 0.4 μm (the second row), Ra = 0.8 μm (the third row), and Ra = 1.6 μm (the fourth row) at a) λ = 405 nm and ϕ_r = 35°, b) λ = 515 nm and ϕ_r = 155°, and c) λ = 671 nm and ϕ_r = 20°.

Fig.6. Normalized mean value of PS and PP images as functions of azimuth angle ϕ_r at incident wavelengths of a) 405 nm, b) 515 nm, and c) 671 nm.

The mean values are calculated for all pixels in these polarized images. For evaluating polarization more precisely, the normalized mean value of the PS and PP images are calculated by a total of PS + PP. Fig.6. specifies the normalized mean value of PS and PP images for different micro-roughnesses as functions of ϕ_r at incident wavelengths 405 nm, 515 nm, 671 nm. In Fig.6.a) and Fig.6.b), the normalized mean values in these polarized images alter smoothly from one azimuth angle to the next at incident wavelengths of 515 nm and 405 nm. However, normalized mean values in Fig.6.c) have continued to decline rapidly at 671 nm wavelength. The observed normalized mean values are fairly dependent on incident wavelength. Furthermore, the polarization states are derived for all standard sheets in terms of azimuth angle. Fig.7. illustrates the mean principal angle for different micro-roughnesses as functions of ϕ_r at incident wavelengths of 405 nm, 515 nm, and 671 nm. We see almost no change to the mean principal angle at 405 nm and 515 nm wavelengths in Fig.7.a) and Fig.7.b). It is difficult to distinguish different types of surface roughness by the mean principal angle. Fig.7.c) apparently shows that the largest deviation from the mean principal angle occurs in the backscattering. This is because backscattering is not only responsive to the micro-roughness, but also involves influence of spatial skew beams, which also vary with micro-roughness.
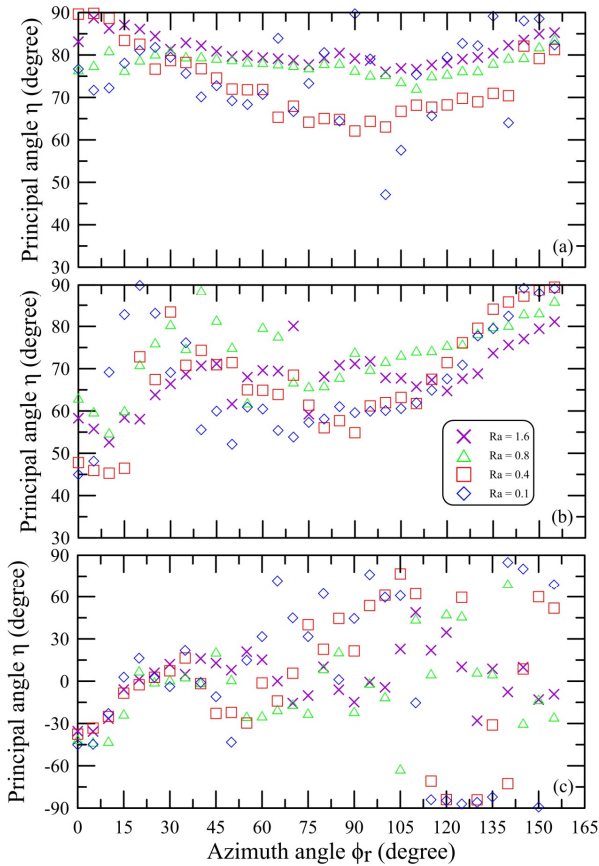

Fig.7. Mean principal angle η as a function of azimuth angle ϕ_r for different micro-roughnesses at incident wavelengths of a) 405 nm, b) 515 nm, and c) 671 nm.
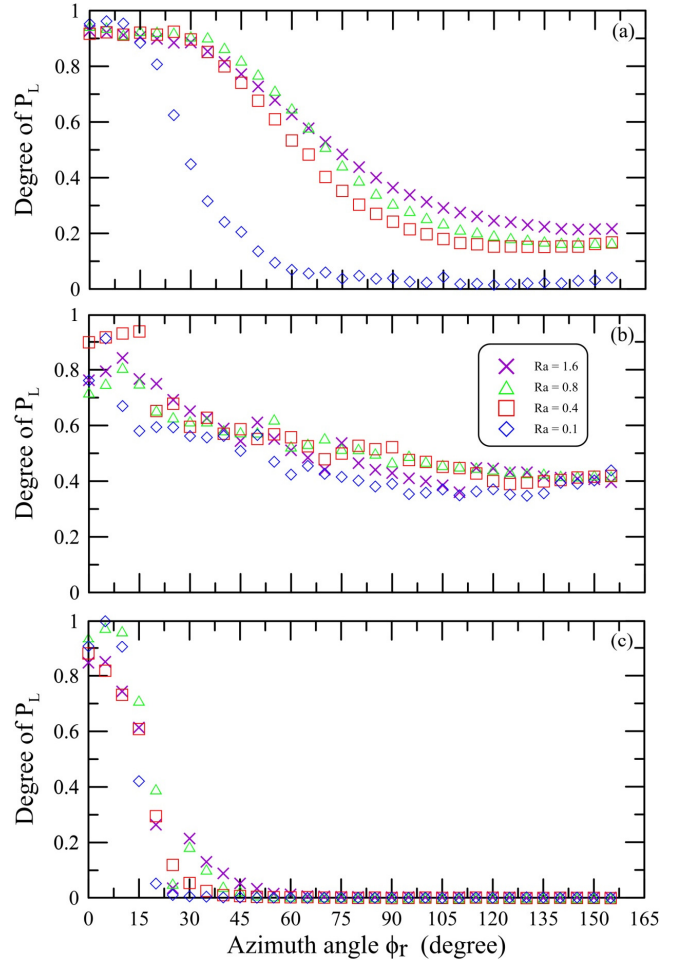

Fig.8. Mean degree of linear polarization P_L as a function of azimuth angle ϕ_r for different micro-roughnesses at incident wavelengths of a) 405 nm, b) 515 nm, and c) 671 nm.

Fig.8. illustrates the P_L as a function of ϕ_r for different micro-roughnesses at incident wavelengths of 405 nm, 515 nm, and 671 nm. The influences of micro-roughness on the polarization of optical scattering for the studied cases are best considered through utilization of Fig.8. These polarized reactions demonstrate the certainty of the facet light-scattering type to some content for different rough surfaces. When the azimuth angle is set appropriately, the degree of linear polarization P_L has critical impact on the definition of micro-roughness. In Fig.8.a), the value of P_L reduces slowly and continues to decrease until $\phi_r = 155°$ for different surface roughnesses. In Fig.8.c), the value of P_L reduces quickly for $\phi_r < 30°$ for all surface roughnesses. These physical phenomena imply that the polarization states of optical scattering supply enough knowledge to discriminate micro-roughness with appropriate wavelength. The surface roughness can be simply specified based on the graph of P_L. The slopes of P_L versus azimuth angle for the curves vary with the micro-roughness value. The value of surface roughness can be related to the slope of P_L for the curves at $\phi_r = 15°$ for 405 nm, $\phi_r = 5°$ for 515 nm, and $\phi_r = 0°$ for 671 nm, respectively. Fig.9. shows the slope, $\Delta P_L / \Delta \phi_r$, as a function of surface micro-roughness at different incident

wavelengths for theoretical approximations with experimental results. The quantitative relationship between the slopes of P_L and surface roughness is well received. The optical scattering ellipsometry is used to remove the effect of the scattering intensity from rough surface and highlight the surface characteristics. The experimental results in Fig.9. indicate that the ellipsometric parameter at appropriate azimuth angle can be utilized to evaluate the unknown value of surface micro-roughness.
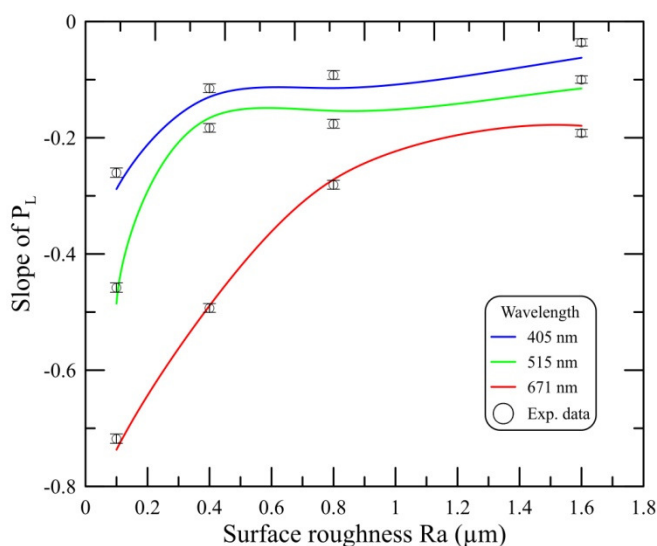

Fig.9. The slope, $\Delta P_L / \Delta \phi_r$, as a function of surface roughness at different incident wavelengths for theoretical approximations with experimental results.

4. CONCLUSION

In this work, we have studied an unusual off-specular measurement based on out-of-plane optical scattering for the characterization of surface micro-roughness. The optical scattering from the surface micro-roughness is measured by the polarized scattering measurement system. Our studies suggest that the polarized imaging technique can be used to observe the key features of micro-roughness. These polarized images of optical scattering from different surface micro-roughness signify the availability of the facet optical scattering model. Through the analysis of polarization images, it is found that the mean degree of linear polarization contributes crucial information to distinguish surface roughness. We have obtained the direct relation between the slope of P_L and the micro-roughness value. The proposed system in this paper can overcome the disadvantage of contact stylus instrument and improve the measurement accuracy. In the future work, we will investigate the effects of multiple light-scattering and interferences for the advance of measurement resolution to nano-scale. Additional work is required to decrease image processing times on the order of a few seconds. We also will proceed with the polarization effect on the unknown values of surface micro-roughness for the optical scattering measurement. The experimental results will be compared with the conventional micro-roughness measurement methods.

REFERENCES

[1] Torrance, K., Sparrow, E. (1967). Theory for off-specular reflection from roughened surfaces. *Journal of the Optical Society of America*, 57, 1105-1114.

[2] Videen, G., Hsu, J., Bickel, W., Wolfe, W. (1992). Polarized light scattered from rough surfaces. *Journal of the Optical Society of America A*, 9, 1111-1118.

[3] Germer, T. (1997). Angular dependence and polarization of out-of-plane optical scattering from particulate contamination, subsurface defects, and surface microroughness. *Applied Optics*, 36, 8798-8805.

[4] Germer, T., Asmail, C., Scheer, B. (1997). Polarization of out-of-plane scattering from microrough silicon. *Optics Letters*, 22, 1284-1286.

[5] Le Bosse, J., Hansali, G., Lopez, J., Dumas, J. (1999). Characterisation of surface roughness by laser light scattering: Diffusely scattered intensity measurement. *Wear*, 224, 236-244.

[6] Tay, C., Quan, C. (2003). A parametric study on surface roughness evaluation of semi-conductor wafers by laser scattering. *Optik*, 114, 1-6.

[7] Germer, T., Asmail, C. (1999). Polarization of light scattered by microrough surfaces and subsurface defects. *Journal of the Optical Society of America A*, 16, 1326-1332.

[8] Jacques, S., Roman, J., Lee, K. (2000). Imaging superficial tissues with polarized light. *Lasers in Surgery and Medicine*, 26, 119-129.

[9] Ghassemi, P., Lemaillet, P., Ramella-Roman, J., Shupp, J., Venna, S., Boisvert, M., Flanagan, K., Jordan, M., Germer, T. (2012). Out-of-plane Stokes imaging polarimeter for early skin cancer diagnosis. *Journal of Biomedical Optics*, 17, 076014.

[10] Torrance, K., Sparrow, E., Birkebak, R. (1966). Polarization, directional distribution, and off-specular peak phenomena in light reflected from roughened Surfaces. *Journal of the Optical Society of America*, 56, 916-925.

[11] Bahar, E., Shi, X. (1998). The scattering and depolarization of electromagnetic waves by random rough surfaces with different scales of roughness: New full wave solutions. *International Journal of Remote Sensing*, 19, 2171-2185.

[12] Shen, Y., Zhu, Q., Zhang, Z. (2003). A scatterometer for measuring the bidirectional reflectance and transmittance of semiconductor wafers with rough surfaces. *Review of Scientific Instruments*, 74, 4885-4892.

[13] Renhorn, I., Boreman, G. (2008). Analytical fitting model for rough-surface BRDF. *Optics Express*, 16, 12892-12898.

[14] Hyde IV, M., Schmidt, J., Havrilla, M. (2009). A geometrical optics polarimetric bidirectional reflectance distribution function for dielectric and metallic surfaces. *Optics Express*, 17, 22138-22153.

[15] Liu, C., Fu, W. (2009). Polarized angular dependence of out-of-plane light-scattering measurements for nanoparticles on wafer. *Optics Communications*, 282, 2097-2103.

[16] Ren, J., Zhao, J. (2010). Measurement of a bidirectional reflectance distribution and system achievement based on a hemi-parabolic mirror. *Optics Letters,* 35, 1458-1460.

[17] Liu, C., Liu, T., Fu, W. (2010). Out-of-plane ellipsometry measurements of nanoparticles on surfaces for thin film coated wafer inspection. *Optics & Laser Technology*, 42, 902-910.

[18] Jin, L., Kasahara, M., Gelloz, B., Takizawa, K. (2010). Polarization properties of scattered light from macrorough surfaces. *Optics Letters,* 35, 595-597.

[19] Renhorn, I., Hallberg, T., Bergstrom, D., Boreman, G. (2011). Four-parameter model for polarization-resolved rough-surface BRDF. *Optics Express*, 19, 1027-1036.

[20] Jin, L., Yamaguchi, K., Watanabe, M., Hira, S., Kondoh, E., Gelloz, B. (2015). Polarization characteristics of scattered light from macroscopically rough surfaces. *Optical Review*, 22, 511-520.

[21] Liu, L., Li, X., Nonaka, K. (2015). Light depolarization in off-specular reflection on submicro rough metal surfaces with imperfectly random roughness. *Review of Scientific Instruments*, 86, 023107.

[22] Collier, C., Hesse, E., Taylor, L., Ulanowski, Z., Penttilä, A., Nousiainen, T. (2016). Effects of surface roughness with two scales on light scattering by hexagonal ice crystals large compared to the wavelength: DDA results. *Journal of Quantitative Spectroscopy & Radiative Transfer*, 182, 225-239.

[23] Doronin, A., Tchvialeva, L., Markhvida, I., Lee, T., Meglinski, I. (2016). Backscattering of linearly polarized light from turbid tissue-like scattering medium with rough surface. *Journal of Biomedical Optics*, 21, 071117.

[24] Grynko, Y., Shkuratov, Y., Förstner, J. (2016). Light scattering by irregular particles much larger than the wavelength with wavelength-scale surface roughness. *Optics Letters,* 41, 3491-3494.

[25] Azzam, R. (2017). Ellipsometry of single-layer antireflection coatings on transparent substrates. *Applied Surface Science*, 421, 271-275.

[26] Fujiwara, H., Fujimoto, S., Tamakoshi, M., Kato, M., Kadowakia, H., Miyadera, T., Tampo, H., Chikamatsu, M., Shibata, H. (2017). Determination and interpretation of the optical constants for solar cell materials. *Applied Surface Science*, 421, 276-282.

[27] Camargo, A., Fellows, C., Lemos, M., Mello, M., Silva, L., Huguenin J. (2019). Roughness measurement of oriented surface by depolarization of scattered light. *Optics and Lasers in Engineering*, 112, 87-92.

[28] Meireles, J., Silva, L., Caetano, D., Huguenin, J. (2012). Effect of metallic surface roughness on the speckle pattern formation at diffraction plane. *Optics and Lasers in Engineering*, 50, 1731-1734.

[29] Fuh, Y., Hsu, K., Fan, J. (2012). Roughness measurement of metals using a modified binary speckle image and adaptive optics. *Optics and Lasers in Engineering*, 50, 312-316.

[30] Gao, Z., Zhao, X. (2012). Roughness measurement of moving weak-scattering surface by dynamic speckle image. *Optics and Lasers in Engineering*, 50, 668-677.

[31] Kim, B., Seo, J. (2015). Measurement of surface roughness of plasma-deposited films using laser speckles. *Applied Surface Science*, 359, 204-208.

[32] Reis, R., Rabal, H., Braga, R. (2016). Light intensity independence during dynamic laser speckle analysis. *Optics Communications*, 366, 185-193.

[33] Cariñe, J., Guzmáncd, R., Torres-Ruiz, F. (2016). Algorithm for dynamic speckle pattern processing. *Optics and Lasers in Engineering*, 82, 56-61.

[34] Ansari, M., Nirala, A. (2016). Biospeckle numerical assessment followed by speckle quality tests. *Optik*, 127, 5825-5833.

[35] Molaei, S. (2016). The measurement of Young's modulus of thin films using secondary laser speckle patterns. *Measurement*, 92, 28-33.

[36] Park, J., Yoon, S., Kwon, T., Park, K. (2017). Assessment of speckle-pattern quality in digital image correlation based on gray intensity and speckle morphology. *Optics and Lasers in Engineering*, 91, 62-72.

[37] Palik, E. (1985). *Handbook of Optical Constants of Solids*. Academic Press.